DOI: 10.24352/UB.OVGU-2018-007 TECHNISCHE MECHANIK, 38, 1, (2018), 73 – 90
submitted: August 29, 2017

Modeling Chemical Reaction Front Propagation by Using an Isogeometric Analysis

A. Morozov[1,3,4], S. Khakalo[2], V. Balobanov[2], A.B. Freidin[3,4,5], W.H. Müller[1], and J. Niiranen[2]

[1]Institute of Mechanics, Faculty of Mechanical Engineering, Berlin Institute of Technology, Einsteinufer 5, 10587 Berlin, Germany
[2]Department of Civil Engineering, School of Engineering, Aalto University, PO Box 12100, 00076 AALTO Rakentajanaukio 4 A, Espoo, Finland
[3]Institute for Problems in Mechanical Engineering of Russian Academy of Sciences, 61 Bolshoy Pr. V.O., St. Petersburg 199178, Russia
[4]Peter the Great St. Petersburg Polytechnic University, Polytechnicheskaya Str. 29, St. Petersburg 195251, Russia
[5]St. Petersburg University, Universitetsky Pr. 28, Peterhof 198504, Russia

We develop a numerical procedure for solving boundary value problems for elastic solids undergoing chemical transformations. The kinetic equation for the reaction front propagation is based on an expression for the chemical affinity tensor, which allows us to study the influence of stresses and strains on the chemical reaction rate and the normal component of the reaction front velocity. Isogeometric analysis provides a high accuracy when finding the normal to the reaction front, and it is applied with the use of Abaqus to a numerical simulation of the front propagation. In order to test and demonstrate the capabilities of the developed procedure a hollow cylinder undergoing a chemical transformation is considered. First, an axially-symmetric problem is solved and a good agreement between numerical simulations and analytical results is demonstrated. Then a case is considered where the initial front configuration does not have axial symmetry. Reaction front acceleration, retardation, and even reaction blocking due to mechanical stresses are investigated.

1 Description of the Problem

During recent decades much attention in the mechanics of deformable solids has been paid to the study of materials, which change their structure due to phase or chemical transformations under thermomechanical actions (see, e. g., Müller et al. (2015) and reference therein). The peculiarity of such studies is their interdisciplinarity where coupled problems of mechanics, physics, and chemistry arise. Some examples come from MEMS (MicroElectroMechanical Systems) and some from microelectronics. Oxidation processes interconnected with crack growth in polycrystalline silicon microscale parts determine the lifetime of MEMS (Muhlstein et al. (2001, 2002); Muhlstein and Ritchie (2003)). Mechanical stresses can retard the oxidation of silicon nanowires (Buttner and M.Zacharias (2006)). Other examples for such interdisciplinary studies are LIBs (Lithium-Ion Batteries) with novel anode materials, such as silicon. The capacity of silicon is about ten times higher than the charge capacity of graphite anodes, which are mostly used (Kasavajjula et al. (2007)). However, the lithiation and de-lithiation with large amounts of Li results in dramatic volumetric changes of 300% in the Si anodes. Unless accommodated by appropriate compensating deformation the large volumetric change generates mechanical stresses, which in turn may affect the diffusion (Yang (2010), Chang et al. (2015)). In addition, recent experimental observation shows (Liu et al. (2012a), McDowell et al. (2013), Liu et al. (2013), Liu et al. (2012b)) that there is a sharp interface between lithiated and unlithiated phases, that the lithiation process may be controlled by an interfacial chemical reaction (Zenga et al. (2016)), and that the chemical reaction rate is affected by mechanical stresses as well (Yang (2010); Cui et al. (2012a); Levitas and Hamed (2013)). As a result, one faces a complex coupled problem of mechanochemistry with a moving chemical reaction front.

Many numerical simulations of the transformation fronts of various natures were made earlier. For the case of phase transformations see, e.g., Finite Element Analysis (FEA) applications in Mueller and Gross (1998, 1999);

Gross et al. (2002); Mueller et al. (2006). Stress field analysis during mimicking the lithiation front propagation in Li-ion batteries was performed by using FE in Jia and Li (2015). A description of the FE simulation of the propagation of a chemical reaction front with the reaction front kinetics being controlled by the chemical affinity tensor was implemented in Freidin et al. (2016).

This paper can be considered as the step of further utilization of the concept of the chemical affinity tensor in a form developed in Freidin (2009, 2013); Freidin et al. (2014); Freidin (2015) for studying stress controlled chemical reaction front propagation. We use a modern powerful numerical method based on IsoGeometric Analysis (IGA) introduced by Hughes et al. (2005). This method can be considered as the "next generation" of the convenient Finite Element Method (FEM), and by virtue of its increasing complexity it has many advantages. A most important one is the use of an exact geometry directly for the calculations. This is definitely good for problems with complex geometries such as shells in geometrically non-linear formulations (Kiendl et al. (2009)). This also makes IGA especially effective for problems that are very sensitive to geometry imperfections, i.e., sliding contact (De Lorenzis et al. (2014)). For example, this method was used effectively in higher gradient theory studies thanks to higher-order continuities of basis functions (see, e.g., Niiranen et al. (2016, 2017b)).

In the context of problems involving moving interfaces, such as phase boundaries or chemical reaction fronts, IGA allows to represent the interface very smoothly, and therefore to calculate the normal vector to each point of the interface with high accuracy. This is especially important for the movement of the interface in the right direction. And, finally, IGA has higher accuracy with less computational effort compared to standard FEA (cf. Morganti et al. (2015)).

The paper is organized as follows. In Section 2 we present a brief overview of the chemical affinity tensor concept and describe how to implement this approach to the modeling of chemical reaction fronts in solids. In Section 3 a short description of the IGA method is given with its advantages for solving problems with propagating internal interfaces. Section 4 contains numerical results for different configurations of a hollow cylinder undergoing chemical transformation. For an analytical solution of the axially symmetric problem, which is used to verify the numerical procedure, we refer to Appendix A. Finally, conclusions are formulated in the last Section 5.

2 Continuum Model

2.1 Chemical Affinity Tensor

A chemical reaction between a solid and a diffusive constituent with a reaction equation

$$n_- \mathrm{B}_- + n_* \mathrm{B}_* \longrightarrow n_+ \mathrm{B}_+ \tag{1}$$

is considered, where where B_-, B_* and B_+ are the chemical formulae of an initial solid constituent, a diffusive constituent , and a transformed solid constituent, respectively; n_-, n_* and n_+ are the stoichiometric coefficients. The reaction is localized at the reaction front, and all of the supplied B_* is consumed by the reaction (Figure 1). For example, in the case of the charging process in LIBs this is the reaction

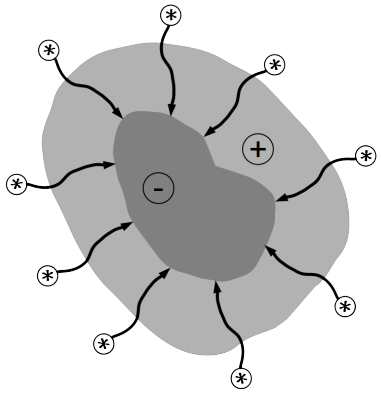

Figure 1: Schematic representation of the chemical reaction in solids

$$\mathrm{Si} + x \cdot \mathrm{Li}^+ + x \cdot \mathrm{e}^- \rightarrow \mathrm{Li}_x\mathrm{Si}. \tag{2}$$

between solid Si and ions of Li which diffuse through $\mathrm{Li}_x\mathrm{Si}$ to the reaction front.

In the case of LIBs lithium ions are large enough to introduce additional deformations in the $\mathrm{Li}_x\mathrm{Si}$ while diffusing. Nevertheless, in order to simplify the analytical solution used for verification of the numerical one we neglect these deformations in this paper and consider a so-called solid skeleton approach. At the same time we take the strains produced by the chemical reaction and the corresponding internal stresses into account.

The Deal-Grove model of the oxidation of silicon (Deal and Grove (1965)) assumes that the reaction rate ω is proportional to the concentration of a diffusive component c with a coefficient of proportionality k_*, which is a reaction rate parameter:

$$\omega = k_* c. \tag{3}$$

A more general description is based on a chemical affinity A equal to the combination of the chemical potentials of the reaction constituents:

$$A = n_- M_- \mu_- + n_* M_* \mu_* - n_+ M_+ \mu_+, \tag{4}$$

where $\mu_\pm$ and μ_* are chemical potentials, and $M_\pm$ and M_* are molar masses of the constituents $B_\pm$ and B_*, respectively (Prigogine and Defay (1954)). Recall that the chemical affinity appears as a thermodynamic force in the derivation of the entropy production $P[S]$ due to a chemical reaction, i.e., as a multiplier to the reaction rate, which is a thermodynamic flux,

$$TP[S] = A\omega, \tag{5}$$

where T is the temperature. This in turn provides a motivation to formulate a kinetic equation for the reaction rate in a form of dependence of the reaction rate on the affinity, $\omega = \omega(A)$. With the chemical affinity, in the case of the reaction between solid and diffusive constituents, the following kinetic equations was considered (Glansdorff and Prigogine (1971)),

$$\omega = k_* c \left[1 - \exp\left(-\frac{A}{RT}\right)\right], \tag{6}$$

where R is the universal gas constant and $k_* c$ represents the partial rate of the direct chemical reaction.

In the case of solid constituents the chemical potentials are no longer scalar but tensorial quantities $\mathbf{M}_\pm$ (see, e.g., the derivations, discussions and references in Grinfeld (1991)) and can be represented by Eshelby energy-momentum tensors (Eshelby stress tensors), divided by the referential mass densities $\rho_\pm$ of $B_\pm$:

$$\mathbf{M}_\pm = f_\pm \mathbf{I} - \frac{1}{\rho_\pm} \mathbf{F}_\pm^\top \cdot \mathbf{S}_\pm, \tag{7}$$

where $f_\pm$ are the specific Helmholtz free energy densities of $B_\pm$, $\mathbf{F}$ is the deformation gradient, $\mathbf{I}$ is the identity tensor and $\mathbf{S}$ is the first Piola-Kirchhoff stress tensor.

Recently, for a chemical reaction (1) between diffusive and solid constituents of arbitrary rheologies, the expression of the chemical affinity tensor was obtained from the mass, energy and linear momentum balances and with the use of the entropy inequality (Freidin (2013, 2015), see also Appendix in Freidin et al. (2014)). It was shown that the entropy production takes the form

$$TP[S] = A_{NN} \omega_N, \tag{8}$$

where ω_N is the reaction rate at the oriented area element with the normal $\mathbf{N}$, and A_{NN} is the normal component of the chemical affinity tensor $\mathbf{A}$ which in the quasistatic case is equal to

$$\mathbf{A} = n_- M_- \mathbf{M}_- + n_* M_* \mu_* \mathbf{I} - n_+ M_+ \mathbf{M}_+, \tag{9}$$

where μ_* is the chemical potential of the diffusive constituent. The expression (9) was obtained earlier for nonlinear elastic solid constituents in Freidin (2009). The tensorial nature of the chemical affinity was also pointed out in Rusanov (2005, 2006).

After replacing the scalar chemical affinity A in Eq. (6) by the normal component of the affinity tensor A_{NN}, the reaction rate becomes:

$$\omega = k_* c \left[1 - \exp\left(-\frac{A_{NN}}{RT}\right)\right]. \tag{10}$$

Then the normal component of the reaction front velocity can be found from the mass balance at the propagating reaction front:

$$W = \frac{n_- M_-}{\rho_-} \omega. \tag{11}$$

In Freidin (2013); Freidin et al. (2014); Freidin (2015) a formula for the normal component of the affinity tensor was presented after using a kinematic compatibility condition and traction continuity across the reaction front. If we assume that the chemical potential of the diffusive constituent is

$$M_*\mu_* = \eta_*(T) + RT\ln\frac{c}{c_*}, \tag{12}$$

where $\eta_*(T)$ is a temperature dependent chemical energy of the diffusive constituent and c_* is a reference concentration, and additionally neglect the input of the pressure of the diffusive constituent into stresses at the reaction front, then in the case of small strains the normal component of the affinity tensor takes the form

$$A_{NN} = \frac{n_-M_-}{\rho_-}\big(w_- - g^3 w_+ + \boldsymbol{\sigma}_\pm : [\![\boldsymbol{\varepsilon}]\!]\big) + n_*\Big(RT\ln\frac{c}{c_*} + \eta_*\Big), \tag{13}$$

where $w_\pm$ are the Helmholtz free energies of the solid constituents per unit volumes of their reference configurations, g is the volume effect of the reaction, square brackets denote the jump of a value across the reaction front $[\![\phi]\!] = \phi_+ - \phi_-$, and $\boldsymbol{\varepsilon}_\pm$ are the strains at the reaction front. Note that from the displacement and traction continuity it follows that the stress $\boldsymbol{\sigma}_\pm$ on any side of the reaction front can be substituted into (13).

The Cauchy stresses are related to the strains via Hooke's law:

$$\boldsymbol{\sigma}_- = \mathbf{C}_- : \boldsymbol{\varepsilon}_-, \quad \boldsymbol{\sigma}_+ = \mathbf{C}_+ : (\boldsymbol{\varepsilon}_+ - \boldsymbol{\varepsilon}^{\mathrm{ch}}), \tag{14}$$

where $\mathbf{C}_\pm$ are the elasticity tensors of the constituents $B_\pm$, $\boldsymbol{\varepsilon}^{\mathrm{ch}} = \varepsilon^{\mathrm{ch}}\mathbf{I}$, $\varepsilon^{\mathrm{ch}} = (g-1)$ is the transformation strain, where $\mathbf{I}$ is the unit tensor. Then the Helmholtz free energy densities are

$$w_- = \eta_-(T) + \frac{1}{2}\boldsymbol{\varepsilon}_- : \mathbf{C}_- : \boldsymbol{\varepsilon}_-, \quad w_+ = \eta_+(T) + \frac{1}{2}\big(\boldsymbol{\varepsilon}_+ - \boldsymbol{\varepsilon}^{\mathrm{ch}}\big) : \mathbf{C}_+ : \big(\boldsymbol{\varepsilon}_+ - \boldsymbol{\varepsilon}^{\mathrm{ch}}\big), \tag{15}$$

where $\eta_\pm(T)$ are the free energy volume densities of the solid constituents in stress-free states (temperature dependent chemical energies of the solid constituents), and the normal component of the chemical affinity tensor can be written as:

$$A_{NN} = \frac{n_-M_-}{\rho_-}\left\{\gamma(T) + \frac{1}{2}\boldsymbol{\sigma}_- : \boldsymbol{\varepsilon}_- - \frac{1}{2}\boldsymbol{\sigma}_+ : (\boldsymbol{\varepsilon}_+ - \boldsymbol{\varepsilon}^{\mathrm{ch}}) + \boldsymbol{\sigma}_- : (\boldsymbol{\varepsilon}_+ - \boldsymbol{\varepsilon}_-)\right\} + n_*RT\ln\frac{c}{c_*}, \tag{16}$$

where the energy parameter γ is determined by chemical energies of the constituents as:

$$\gamma = \eta_- - g\eta_+ + \frac{\rho_-}{n_-M_-}n_*\eta_*. \tag{17}$$

2.2 Mechanical Problem and Representation A_{NN} through the Strains or Stresses on One Side of the Reaction Front

As mentioned above, for simplicity sake we neglect the influence of the pressure of the diffusive constituent on the stress state. Then the equilibrium equation to find the stress state reads:

$$\nabla \cdot \boldsymbol{\sigma} = \mathbf{0}, \tag{18}$$

and the boundary conditions at the outer surface Γ of a body and conditions at the reaction front Γ_{ch} are

$$\begin{aligned} &\mathbf{u}|_{\Gamma_1} = \mathbf{u_0}, \quad \boldsymbol{\sigma}\cdot\mathbf{N}|_{\Gamma_2} = \mathbf{t_0}, \\ &[\![\mathbf{u}]\!]|_{\Gamma_{\mathrm{ch}}} = \mathbf{0}, \quad [\![\boldsymbol{\sigma}]\!]\cdot\mathbf{N}|_{\Gamma_{\mathrm{ch}}} = \mathbf{0}, \end{aligned} \tag{19}$$

where $\Gamma_1 \cup \Gamma_2 = \Gamma$, $\mathbf{u_0}$ and $\mathbf{t_0}$ are the prescribed displacement and traction, respectively.

From the displacement and traction continuity at the reaction front it follows that if the constitutive equations of contacting materials have Hooke's form (14) then the jumps of strains and stresses can be expressed as functions of strains or stresses on one side of the reaction front (Kunin (1983)):

$$[\![\boldsymbol{\varepsilon}]\!] = -\mathbf{K}_\mp(\mathbf{N}) : \mathbf{q}_\pm, \quad [\![\boldsymbol{\sigma}]\!] = \mathbf{S}_\mp(\mathbf{N}) : \mathbf{m}_\pm, \tag{20}$$

where the tensors $\mathbf{q}$ and $\mathbf{m}$ are linearly related to strains and stresses at the reaction front, and the coefficients of the linear dependencies are the jumps in elasticity or compliance tensors, and transformation strain:

$$\begin{gathered}\mathbf{q}_{\pm}=[\![\mathbf{C}]\!]:\boldsymbol{\varepsilon}_{\pm}-\mathbf{C}_{+}:\boldsymbol{\varepsilon}^{\mathrm{ch}},\quad \mathbf{m}_{\pm}=[\![\mathbf{B}]\!]:\boldsymbol{\sigma}_{\pm}+\boldsymbol{\varepsilon}^{\mathrm{ch}},\\ \mathbf{K}_{\mp}(\mathbf{N})=\{\mathbf{N}\otimes\mathbf{G}_{\mp}(\mathbf{N})\otimes\mathbf{N}\}^{s},\quad \mathbf{G}_{\mp}(\mathbf{N})=(\mathbf{N}\cdot\mathbf{C}_{\mp}\cdot\mathbf{N})^{-1},\\ \mathbf{S}_{\mp}(\mathbf{N})=\mathbf{C}_{\mp}:\mathbf{K}_{\mp}(\mathbf{N}):\mathbf{C}_{\mp}-\mathbf{C}_{\mp},\ \mathbf{B}_{\pm}=\mathbf{C}_{\pm}^{-1},\end{gathered}\tag{21}$$

upper and lower scripts "+" and "−" in the relationships correspond to each other, $\mathbf{G}(\mathbf{N})$ is the Fourier transform of Green's tensor, the inverse of the acoustic tensor, s means symmetrization: $K_{ijkl}=N_{(i}G_{j)(k}N_{l)}$.

From (16) and (20) it follows that the "mechanical" part of the normal component of the chemical affinity tensor can be expressed through strains or stresses on one side of the front, similar to the expressions of the jump of the normal component of the Eshelby stress tensor across the interface in the case of phase transformations (Kubanov and Freidin (1988); Freidin (1989), see also Morozov and Freidin (1998); Freidin (2007)). If the chemical potential of the diffusive constituent is given by (12) then from (16) and (20) it follows that

$$A_{NN}=\frac{n_{-}M_{-}}{\rho_{-}}\left\{\gamma+\frac{1}{2}\,\boldsymbol{\varepsilon}^{\mathrm{ch}}\colon\mathbf{C}_{+}:\boldsymbol{\varepsilon}^{\mathrm{ch}}+\frac{1}{2}\,\boldsymbol{\varepsilon}_{\pm}\colon[\![\mathbf{C}]\!]:\boldsymbol{\varepsilon}_{\pm}-\boldsymbol{\varepsilon}_{\pm}\colon\mathbf{C}_{+}:\boldsymbol{\varepsilon}^{\mathrm{ch}}\pm\frac{1}{2}\,\mathbf{q}_{\pm}\colon\mathbf{K}_{\mp}\left(\mathbf{N}\right):\mathbf{q}_{\pm}\right\}$$
$$+n_{*}RT\ln\frac{c}{c_{*}},\tag{22}$$

$$=\frac{n_{-}M_{-}}{\rho_{-}}\left\{\gamma-\frac{1}{2}\,\boldsymbol{\sigma}_{\pm}\colon[\![\mathbf{B}]\!]\colon\boldsymbol{\sigma}_{\pm}-\boldsymbol{\sigma}_{\pm}\colon\boldsymbol{\varepsilon}^{\mathrm{ch}}\pm\frac{1}{2}\,\mathbf{m}_{\pm}\colon\mathbf{S}_{\mp}\left(\mathbf{N}\right)\colon\mathbf{m}_{-}\pm\right\}+n_{*}RT\ln\frac{c}{c_{*}}.\tag{23}$$

The above representations allow to compute A_{NN} directly through strains or stresses without recalculation of strains into stresses or vice versa.

2.3 Velocity of the Reaction Front

The chemical transformation involves two processes (Figure 2), bulk diffusion of the constituent B_{*} through material B_{+}, and a chemical reaction between the constituents B_{*} and B_{-} at the reaction front Γ_{ch}.

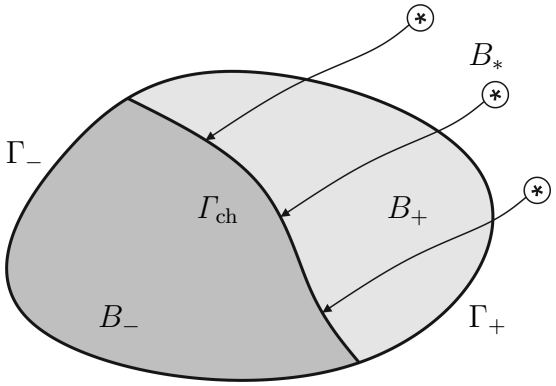

Figure 2: Schematic representation of the chemical transformation process

By the solid skeleton approach the tensors $\mathbf{M}_{\pm}$ in the expression for the chemical affinity tensor do not depend on the concentration c of the constituent B_{*}. Then the equilibrium concentration c_{eq} of the diffusive constituent can be introduced, such that for stresses acting at the reaction front we have

$$A_{NN}(c_{\mathrm{eq}})=n_{-}M_{-}M_{NN}^{-}+n_{*}M_{*}\mu_{*}(c_{\mathrm{eq}},T)-n_{+}M_{+}M_{NN}^{+}=0,\tag{24}$$

where $M_{NN}^{\pm}=\mathbf{N}\cdot\mathbf{M}_{\pm}\cdot\mathbf{N}$. This in turn leads to the representation of of the normal component of the chemical through the difference of chemical potentials of the diffusive constituent calculated at the current and equilibrium concentrations (Vilchevskaya and Freidin (2009, 2013), see also Freidin et al. (2014); Freidin (2015)):

$$A_{NN}=n_{*}M_{*}\left(\mu_{*}(c,T)-\mu_{*}(c_{\mathrm{eq}},T)\right),\tag{25}$$

where the concentration c at the reaction front is obtained from the solution of the diffusion problem, and c_{eq} is to be found from Eq. (24).

If the the assumption (12) is made about the chemical potential of the diffusive constituent, then A_{NN} can be taken in the form (22) or (23) at strains or stresses which act at the reaction front and, in turn, are to be found from the solution of the mechanical problem. For example, if strains are found on one side of the reaction front, then

$$c_{\rm eq} = c_* \exp\left(-\frac{\chi(\boldsymbol{\varepsilon}, T)}{RT}\right), \tag{26}$$

where $\chi(\boldsymbol{\varepsilon}, T)$ is the "mechanical" part of A_{NN}:

$$\chi(\boldsymbol{\varepsilon}, T) = \frac{n_- M_-}{\rho_-}\left(\gamma(T) + \frac{1}{2}\boldsymbol{\varepsilon}^{\rm ch} : \mathbf{C}_+ : \boldsymbol{\varepsilon}^{\rm ch} + \frac{1}{2}\boldsymbol{\varepsilon}_\pm : [\![\mathbf{C}]\!] : \boldsymbol{\varepsilon}_\pm \right. \\ \left. - \boldsymbol{\varepsilon}_\pm : \mathbf{C}_+ : \boldsymbol{\varepsilon}^{\rm ch} \pm \frac{1}{2}\mathbf{q}_\pm : \mathbf{K}_\mp(\mathbf{N}) : \mathbf{q}_\pm\right). \tag{27}$$

If both concentrations, c and $c_{\rm eq}$, are found then

$$A_{NN} = n_* RT \ln\frac{c}{c_{\rm eq}}. \tag{28}$$

Substituting this expression into Eq. (10) results in the expression for the reaction rate

$$\omega = k_* c\left\{1 - \left(\frac{c_{\rm eq}}{c}\right)^{n_*}\right\}. \tag{29}$$

If $n_* = 1$ then the reaction rate reads:

$$\omega = k_*(c - c_{\rm eq}), \tag{30}$$

and the normal component of the reaction front velocity can be found by substituting Eq. (30) into Eq. (11):

$$W = \frac{n_- M_-}{\rho_-} k_*(c - c_{\rm eq}). \tag{31}$$

2.4 Diffusion Problem

In order to find the concentration of the diffusive constituent B_* one has to solve a diffusion problem. For simplicity of further analytical solutions we assume a simple Fick's law of diffusion. In particular the influence of mechanical stresses on the diffusion flux is neglected. We also assume that diffusion rate is much higher then the chemical reaction rate and consider stationary diffusion. Time affects the spatial distribution of B_* only through the position of the reaction front. Then the corresponding diffusion equation can be written as the Laplace equation:

$$\Delta c = 0, \tag{32}$$

which is to be solved in the domain v_+ occupied by the material B_+.

A boundary condition on the moving reaction front $\Gamma_{\rm ch}$ follows from equalizing the consumption of the diffusive constituent by the chemical reaction and its flux:

$$D\mathbf{N}\cdot\nabla c + n_*\omega = 0 \quad \text{at} \quad \Gamma_{\rm ch}, \tag{33}$$

where D is the diffusivity of B_* through the material B_+, and $\mathbf{N}$ is the normal to the reaction front outward to v_+.

By (29), the condition (33) can be rewritten as

$$D\mathbf{N}\cdot\nabla c + n_* k_* c\left\{1 - \left(\frac{c_{\rm eq}}{c}\right)^{n_*}\right\} = 0 \quad \text{at} \quad \Gamma_{\rm ch}. \tag{34}$$

If $n_* = 1$ then the condition at the reaction front takes the form

$$D\mathbf{N}\cdot\nabla c + k_*(c - c_{\rm eq}) = 0 \quad \text{at} \quad \Gamma_{\rm ch}. \tag{35}$$

The second boundary condition for the diffusion problem concerns the supply at the outer surface Γ_+ of the domain v_+ through which the diffusive constituent enters the domain. In this context a condition, which prescribes the flux through the outer surface, is used:

$$D\mathbf{N}\cdot\nabla c - \alpha(c_* - c) = 0 \quad \text{at} \quad \Gamma_+, \tag{36}$$

where α is the surface mass transfer coefficient, c_* is the diffusive constituent solubility in the transformed material B_+, and the normal is outward to v_+.

2.5 A General Procedure of the Simulation of the Reaction Front Kinetics

In order to simulate reaction front kinetics one has to go through the following steps (Freidin et al. (2016)):

- Find the stresses and strains at the reaction front;
- Find the equilibrium concentration c_{eq} from $A_{NN} = 0$;
- Solve the diffusion problem and calculate the concentration c of the diffusive constituent at the reaction front Γ_{ch};
- Calculate the normal component of the reaction front velocity W;
- Assign an increment $\triangle u = W\Delta t$ to each point of the reaction front in the normal direction and find a new position of the front, where Δt is the time increment;
- Repeat the procedure with a new position of the chemical reaction front.

3 Numerical Simulation

We consider a quasi-static model in the numerical simulation. In our approach we perform the aforementioned steps and find a value of the normal component of reaction front velocity W. Then by choosing a reasonably small time increment Δt we apply a displacement $\triangle u$ to every point of the reaction front. One of the key points in order to simulate the propagation of the chemical front accurately is to guarantee a smooth transition of the normal vector $\mathbf{N}$ at the reaction front. Traditional finite elements have kinks at the connecting nodes, which prohibits a unique determination of the normal. This is one of the main reasons for implementing isogeometric analysis. By using Non-Uniform Rational B-Splines (NURBS) as basis functions we calculate with high accuracy the direction of the normal vector for each curve in the geometry model, and particularly for the chemical reaction front.

One should note that notation for letters describing curves, surfaces, basis functions etc. in the following section was introduced by Hughes et al. (2005) and is generally accepted. All these letters are defined in the following text and are related to the IGA background section only. They must not be confused with similar symbols in other sections of this paper.

3.1 Isogeometric Analysis Background

As it was mentioned above isogeometric analysis was introduced by Hughes et al. (2005). The main idea is to connect CAD (Computer Aided Design) and CAE (Computer Aided Engineering), and in particular FEA closely in industrial engineering processes. This can be achieved by replacing standard basis functions of classical finite elements by functions that are highly utilized in CAD software, such as B-splines and NURBS. An advantage of this approach is that we use the exact CAD geometry directly in the calculations.

NURBS functions are built from B-splines, which are defined recursively in parameter space by the Cox-de Boor recursion formula (Cox (1971), De Boor (1972)),

$$\begin{aligned} p = 0: \qquad N_{i,0}(\xi) &= \begin{cases} 1, & \text{if } \xi_i \le \xi < \xi_{i+1} \\ 0, & \text{otherwise} \end{cases} \\ p = 1, 2... : N_{i,p}(\xi) &= \frac{\xi - \xi_i}{\xi_{i+p} - \xi_i} N_{i,p-1}(\xi) + \frac{\xi_{i+p-1} - \xi}{\xi_{i+p+1} - \xi_{i+1}} N_{i,p-1}(\xi), \end{aligned} \tag{37}$$

where p is a polynomial order of the B-spline, ξ_i are members of the predefined knot vector Ξ. A linear combination of B-spline basis functions gives a piecewise-polynomial B-spline curve,

$$\mathbf{C}(\xi) = \sum_{i=1}^{n} N_{i,p}(\xi)\mathbf{B_i}, \tag{38}$$

where $\mathbf{B_i}$ are coordinates of control points. An example of second order basis functions and a two-element quadratic B-spline curve is shown in Figure 3.

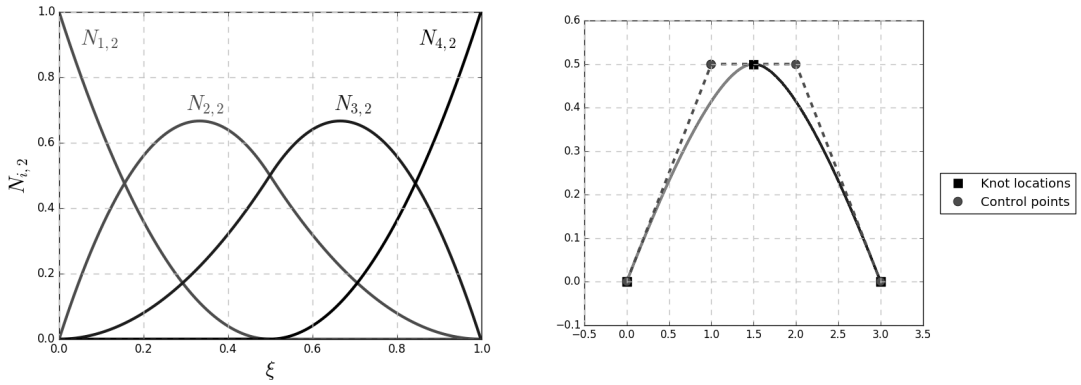

Figure 3: B-spline second order basis functions (left) and two-element quadratic curve (right) for the knot vector $\Xi = \{0, 0, 0, 0.5, 1, 1, 1\}$

In order to build a NURBS curve we have to introduce a weight function,

$$W(\xi) = \sum_{i=1}^{n} N_{i,p}(\xi) w_i, \tag{39}$$

where w_i is the weight of i^{th} control point $\mathbf{B_i}$. Then the NURBS curve is defined by

$$\mathbf{C}(\xi) = \sum_{i=1}^{n} \frac{N_{i,p}(\xi) w_i}{W(\xi)} \mathbf{B}_i. \tag{40}$$

We consider a 2D planar problem. Hence we use NURBS surfaces that are defined analogously by bases, $N_{i,p}$ and $M_{j,q}$, and weight functions, W, weights, $w_{i,j}$, and a control net, $\mathbf{B}_{i,j}$:

$$\begin{aligned} W(\xi, \eta) &= \sum_{i=1}^{n} \sum_{j=1}^{m} N_{i,p}(\xi) M_{j,q}(\eta) w_{i,j}, \\ \mathbf{S}(\xi, \eta) &= \sum_{i=1}^{n} \sum_{j=1}^{m} \frac{N_{i,p}(\xi) M_{j,q}(\eta) w_{i,j}}{W(\xi, \eta)} \mathbf{B}_{i,j}. \end{aligned} \tag{41}$$

With these basis functions and by using a variational formulation (Hughes et al. (2005)) we can form the global system equation of the standard form for a static problem:

$$\mathbf{K}\mathbf{u} = \mathbf{f}, \tag{42}$$

where $\mathbf{K}$ is the global stiffness matrix, $\mathbf{u}$ stands for the unknown vector of global degrees of freedom and $\mathbf{f}$ denotes the global force vector.

The implementation of the method described above was accomplished with the aid of the commercial finite-element software Abaqus. In particular, we created user element subroutines in order to perform an isogeometric analysis by using the standard finite-element analysis procedure as described in Khakalo and Niiranen (2017). Furthermore, the commercial software Abaqus was used for solving this matrix problem and for postprocessing the results.

3.2 Algorithm for Numerical Simulation of the Reaction Front Propagation

Following the sequence of steps listed in Section 2.5 we split the problem into three steps for each iteration, as shown in Figure 4. Since we consider a linear elastic problem with a solid skeleton approach, the mechano-chemical problem can be decoupled. In this particular case the elasticity and the diffusion problem are solved separately in the numerical procedure, one after another. In addition, the linearity of the model makes it possible to present all results in the reference configuration. In all following examples we assume the existence of some thin initially transformed material layer. First, we solve an elasticity problem governed by Eq. (18) with boundary

conditions (19) in order to find the stresses and strains at the reaction front. By substituting these values into the expression for the normal component of the affinity tensor (22) or (23) we obtain an equilibrium concentration of the diffusive constituent by Eq. (26).

Second, we solve the diffusion problem governed by the Laplace equation (32) with the boundary conditions (34) and (35) where we substitute the value of c_{eq}. As a result we get a concentration of the diffusive constituent at the reaction front.

Finally, we substitute all relevant values found in the previous steps into the expression (31) for the normal component of the reaction front velocity. In order to define the value of the interface front displacement in the numerical procedure we solve Eq. (31) with an explicit integration scheme,

$$\rho_{i+1} = \rho_i - \frac{n_- M_-}{\rho_-} k_* \left(c(\rho_i) - c_{\mathrm{eq}}(\rho_i) \right) \Delta t, \tag{43}$$

where the index i refers to the previous iteration and Δt is a fixed value for the time increment. By choosing a reasonably small time increment, whose value we define from the numerical experiment, we obtain a displacement for the chemical front,

$$u_{\mathrm{ch}} = \rho_{i+1} - \rho_i, \tag{44}$$

which we use as a boundary condition for the following problem. Since IGA uses displacements of control points as degrees of freedom which, in general, do not have interpolatory properties, we cannot move the internal front directly. In order to apply this displacement and re-mesh the domain appropriately, we solve the following (third) problem of classic elasticity:

We consider two phases as separate domains (recall Figure 2), which have a common boundary Γ_{ch}, and apply movements u_{ch} on this boundary as non-homogeneous Dirichlet boundary conditions. This widespread technique for imposing such kind of boundary conditions weakly is known as Nitsche's method (see Juntunen and Stenberg (2009) and references therein). We use a modification of this approach based on results for interfaces described in Hansbo (2005). All other (external) boundaries remain unchanged due to strongly imposed homogeneous Dirichlet boundary conditions.

Summarizing all of the above-mentioned information, as the result of the analysis on the third step, we get the new coordinates of control points, which determine the geometrical position of the reaction front and provide a fine and uniformly structured distribution of the mesh inside of the domain. We use this information as the initial model configuration for the next iteration. We trace the position of the reaction front and manually stop the procedure when the chemical reaction front intersects the boundary of the body. This is done in order to avoid a numerical singularity caused by zero or negative area of the mesh element.

Considering that the coupled problem of mechanochemistry is split and solved as a set of a linear elastic and of a diffusion problem, we refer to Hughes et al. (2005) for the elastic problem and to Manni et al. (2011) for advection-diffusion problems as far as the convergence analysis of isogeometric methods is concerned. For IGA of higher order elasticity problems, theoretical error estimate formulations and optimal convergence results we refer to Niiranen et al. (2016); Niiranen and Niemi (2017); Niiranen et al. (2017a,b).

4 Examples

We consider a hollow cylinder undergoing a chemical reaction (Figure 5). To demonstrate how IGA works we consider three plane-strain cases: a circular cylinder with a circular hole and circular reaction front, a circular cylinder with a circular hole and elliptic initial reaction front, and a circular cylinder with an elliptic hole and circular initial reaction front. Due to the symmetry of the problems we analyze only one quarter of the cylinder's cross-section and apply symmetry boundary conditions at the cut edges.

Material properties and model parameters are given in Table 1. Elastic properties are given for Si and lithiated Si (Cui et al. (2012b)). Due to a lack of experimental data (to the best knowledge of the authors), model parameters were kept within reasonable values according to Freidin et al. (2016). The parameter γ was varied in order to obtain different effects for chemical front propagation.

The isogeometric model used for numerical simulation is shown in Figure 6. For the calculations we used NURBS basis functions of $p = 5$th polynomial order and 128 IGA elements to represent the geometry.

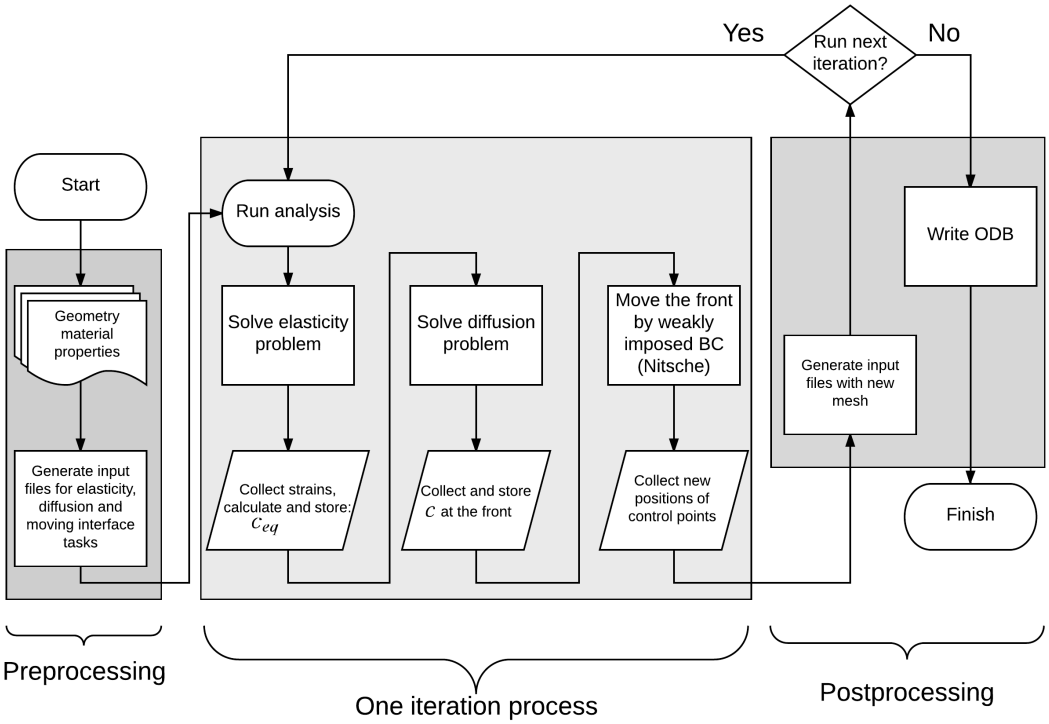

Figure 4: Framework of the numerical procedure

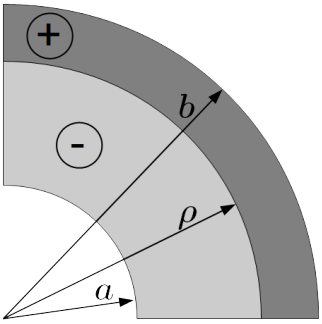

Figure 5: Quarter of a hollow cylinder consisting of two materials

4.1 Axially Symmetric Problem for the Hollow Cylinder

Axially symmetric problems for chemical transformations in a solid cylinder and in an infinite body with a cylindrical hole were studied earlier analytically in Vilchevskaya and Freidin (2013). In the present paper a chemical transformation of a hollow cylinder is considered with a reaction starting from the outer surface. In order to validate the developed isogeometric procedure we compare the results of numerical simulation with an analytical solution (see Appendix A). Inner and outer radii of the cylinder are $a = 5\,\mathrm{mm}$ and $b = 10\,\mathrm{mm}$; the position of the initial reaction front is a circle of the radius $\rho = 9\,\mathrm{mm}$.

The result of the numerical simulation of the reaction front propagation is presented in Figure 7 as reaction front radius value versus number of iterations. First, note that an originally circular reaction front keeps its circular shape during the propagation without any additional artificial constraints, and the result of the numerical simulation – the dependence of the front radius ρ on time – agrees perfectly with the dependence obtained from the analytical solution that follows from the integration of the equation

$$\frac{\mathrm{d}\rho}{\mathrm{d}t} = -\frac{n_- M_-}{\rho_-} k_* \left(c(\rho) - c_{\mathrm{eq}}(\rho)\right), \tag{45}$$

where c_{eq} depends on ρ through the dependence of strains at the front on ρ (see Appendix A).

	Material “−”	Material “+”
E, GPa	166	59
ν	0.22	0.22
$\varepsilon^{\mathrm{ch}}$	–	0.08
D, mm^2/s	10^{-1}	
$k_* c_*$, $\mathrm{mol}/\mathrm{mm}^2\mathrm{s}$	10^{-2}	
γ, J/mm^3	50	

Table 1: Material properties and parameters used in numerical simulation

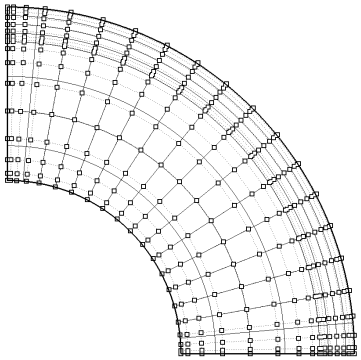

Figure 6: Geometry, created by NURBS curves, which is used for numerical simulation

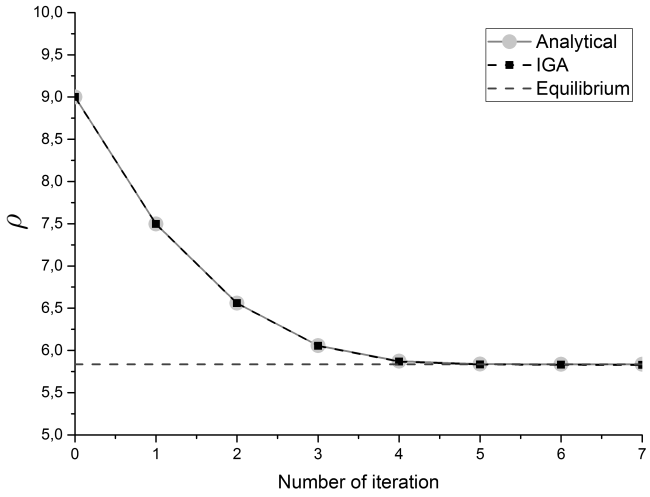

Figure 7: Reaction front kinetics for axially symmetric problem

Second, it can be seen that the front velocity decreases as the front propagates, and at a chosen set of parameters the front almost stops when it reaches a certain radius. This means that the input of stresses in the affinity tensor becomes compatible with the input of chemical energies, and even the diffusion, which continues delivering the constituent B_* to the front, cannot cope with this input because the diffusion flux also decreases. As a result the driving force practically becomes zero and the chemical reaction is nearly blocked, in other words, chemical equilibrium is approached. This result of numerical simulations corresponds to the analytical observation of the case when equilibrium radius $\rho_* \in (a, b)$ exists such that at the reaction front $\chi = 0$ and, thus, $c_{eq}(\rho_*) = c_*$ and $c(\rho)$ becomes constant equal to c_* (see Appendix A).

4.2 Hollow Cylinder with an Elliptic Initial Reaction Front

The next configuration considered is the same hollow cylinder, but with an initially elliptical reaction front with semi-major axis $\mathrm{R_a} = 9\,\mathrm{mm}$ and semi-minor axis $\mathrm{R_b} = 8\,\mathrm{mm}$ (Figure 8, left). In order to avoid stability issues near the equilibrium reaction front, we increase the parameter γ up to $150\,\mathrm{J}/\mathrm{mm}^3$. In this case the equilibrium

reaction front cannot be reached, because it is outside of the body.

The results of the numerical simulations of the reaction front propagation are presented in Figure 9 which shows values for the semi-axes $\mathrm{R_a}$ and $\mathrm{R_b}$ versus the number of iterations. One can conclude that an initially elliptic chemical reaction front tends to become circular during propagation in a cylinder with a circular hole in the center.

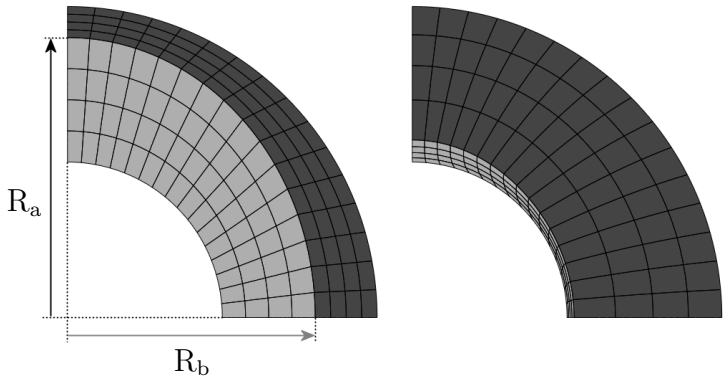

Figure 8: Initial (left) and final (right) position of the reaction front in hollow cylinder with an elliptic initial reaction front

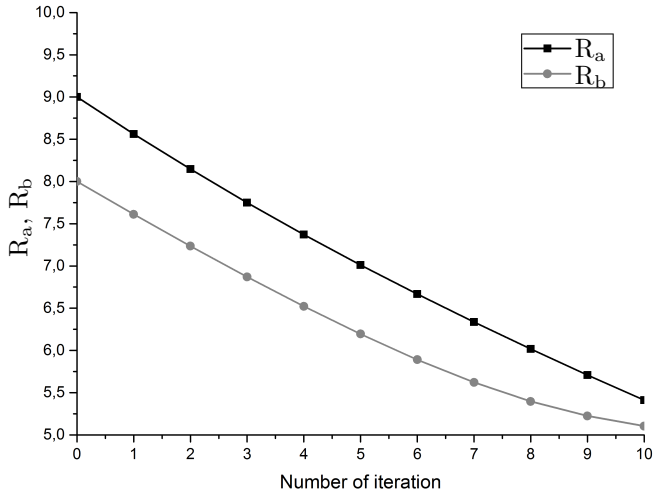

Figure 9: Reaction front kinetics in hollow cylinder with initially elliptic transformed layer

4.3 Cylinder with Elliptical Hole and Circular Initial Reaction Front

The last example is a cylinder with an elliptical hole. The initial reaction front is a circle of the radius $\rho = 9\,\mathrm{mm}$. The ellipse has a semi-minor axis $a_1 = 2\,\mathrm{mm}$ and semi-major axis $a_2 = 5\,\mathrm{mm}$ (Figure 10, left). The parameter $\gamma = 150\,\mathrm{J/mm^3}$ was chosen as in the previous example. The results of the numerical simulation of the reaction front propagation are presented in Figure 11, which shows values of the semi-axes $\mathrm{R_a}$ and $\mathrm{R_b}$ of the reaction front versus the number of iterations.

5 Conclusions and Discussions

In this work we developed a numerical approach to studying the influence of stresses and strains on chemical reaction front propagation. With the use of the concept of a chemical affinity tensor as a theoretical framework, we developed a numerical procedure based on the IGA method, which, to our knowledge, was used for the first time in elasticity problems with moving internal interfaces. We implemented IGA by using Abaqus subroutines. The numerical procedure was validated by an analytical solution for the axially symmetric problem and its effectiveness was confirmed by the approbation for other geometries.

Due to the linearity of the elastic problem and with the assumption of the solid skeleton approach we were able to

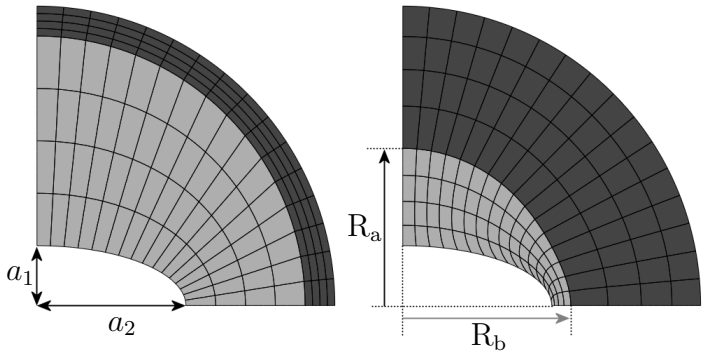

Figure 10: Initial (left) and final (right) position of the reaction front in hollow cylinder with an elliptic hole and circular initial reaction front

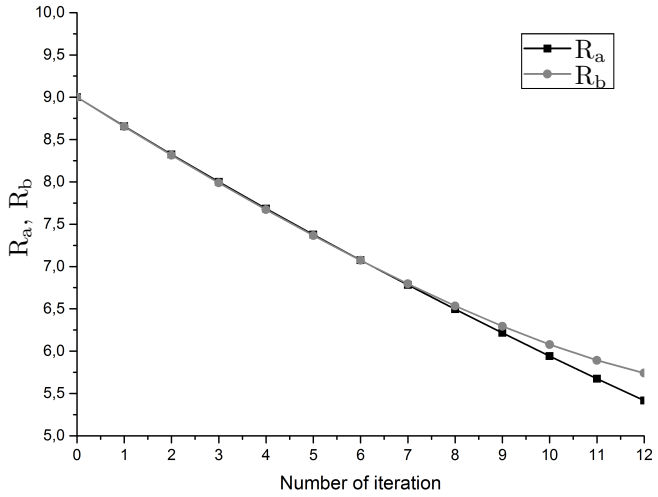

Figure 11: Reaction front kinetics in hollow cylinder with elliptic hole

decouple diffusion and elasticity problems and project all the solutions on the reference configuration. In order to use the proposed procedure for nonlinear elasticity problems or to take a dependency of diffusion on stresses into account, one has to introduce a distinction between the reference and the actual configuration in both analytical and numerical models suitably.

The aforementioned assumptions gave us an opportunity to split the diffusion and the elastic problem also in the numerical procedure and to represent the reaction front propagation in the reference configuration. Since in IGA we cannot move the internal front directly, we used the Nitsche method to move the interface and introduced one more elasticity problem to each iteration in the numerical procedure. Moving the interface is performed on the meshed domain; this is why we had to trace its position and manually stop the numerical procedure when the reaction front reaches one of the external boundaries in order to avoid numerical singularities due to negative volume elements. If we wish to consider a fully reacted solid, we have to add a mesh topology changing procedure.

6 Acknowledgements

S. Khakalo, V. Balobanov and J. Niiranen have been supported by Academy of Finland through the project *Adaptive isogeometric methods for thin-walled structures* (decision numbers 270007, 273609, 304122). Access and licenses for the commercial FE software Abaqus have been provided by CSC IT Center for Science (www.csc.fi).

A. Morozov, A.B. Freidin and W.H. Müller appreciate the support of DFG/RFFI grants (No. MU 1752/47-1 and 17-51-12055).

A.B. Freidin also appreciates the support of Russian Foundation for Basic Research (Grant No. 16-01-00815).

A. Morozov wants to acknowledge funding of his Ph.D. stipend through TU Berlin within the partnership framework with Peter the Great St. Petersburg Polytechnic University.

A Reaction Front Propagation in a Hollow Cylinder. Analytical Solution

We consider the plane strain problem for the hollow cylindrical tube (Figure 5). With given internal and external radii, a and b, respectively, we assume that the reaction front initial position between materials B_+ and B_- is a cylindrical surface of the radius ρ. In a present problem we assume that the transformation strain is plane:

$$\boldsymbol{\varepsilon}^{\mathrm{ch}} = \frac{1}{2}\varepsilon^{\mathrm{ch}}(\mathbf{e}_r \otimes \mathbf{e}_r + \mathbf{e}_\phi \otimes \mathbf{e}_\phi), \tag{46}$$

where $\boldsymbol{e}_r$ and $\boldsymbol{e}_\phi$ are the unit vectors of the cylindrical coordinates, and solid constituents are linear elastic and isotropic:

$$\boldsymbol{\sigma}_- = \mathbf{C}_- : \boldsymbol{\varepsilon}_-, \quad \boldsymbol{\sigma}_+ = \mathbf{C}_+ : (\boldsymbol{\varepsilon}_+ - \boldsymbol{\varepsilon}^{\mathrm{ch}}), \tag{47}$$

$$\mathbf{C}_\pm = \lambda_\pm \mathbf{I} \otimes \mathbf{I} + 2\mu_\pm {}^4\mathbf{I}, \tag{48}$$

where $\lambda_\pm$ and $\mu_\pm$ are Lamé parameters, ${}^4\mathbf{I}$ is the forth rank unit tensor.

1.1 Elasticity Problem and Equilibrium Concentration

In order to find the stresses and strains at the reaction front we use the equilibrium equation, which in the case of axial symmetry takes the form

$$\frac{\mathrm{d}\sigma_r}{\mathrm{d}r} + \frac{\sigma_r - \sigma_\phi}{r} = 0 \tag{49}$$

with boundary conditions

$$\sigma_r(a) = 0, \quad \sigma_r(b) = 0, \quad [\![u(\rho)]\!] = 0, \quad [\![\sigma_r(\rho)]\!] = 0. \tag{50}$$

The radial displacement is given by the Lamé solution:

$$u_\pm(r) = A_\pm r + \frac{B_\pm}{r}, \tag{51}$$

and the strains can be found through

$$\varepsilon_r^\pm(r) = \frac{\mathrm{d}u_\pm(r)}{\mathrm{d}r} = A_\pm - \frac{B_\pm}{r^2}, \qquad \varepsilon_\phi^\pm(r) = \frac{u_\pm(r)}{r} = A_\pm + \frac{B_\pm}{r^2}. \tag{52}$$

Four unknown constants $A_\pm$ and $B_\pm$ can be found from the boundary conditions (50):

$$\begin{aligned}
B_- &= \frac{\varepsilon^{\mathrm{ch}}}{2}\left(\frac{1}{\rho^2} + \frac{\mu_-}{\lambda_- + \mu_-}\frac{1}{a^2} - \frac{\mu_-}{\mu_+}\frac{b^2(\rho^2 - a^2)}{a^2(\rho^2 - b^2)}\left(\frac{1}{\rho^2} + \frac{\mu_+}{\lambda_+ + \mu_+}\frac{1}{b^2}\right)\right)^{-1}, \\
B_+ &= \frac{\mu_-}{\mu_+}\frac{b^2(\rho^2 - a^2)}{a^2(\rho^2 - b^2)}B_-, \\
A_- &= \frac{\mu_-}{\lambda_- + \mu_-}\frac{B_-}{a^2}, \\
A_+ &= \frac{\mu_+}{\lambda_+ + \mu_+}\frac{B_+}{b^2} + \frac{\varepsilon^{\mathrm{ch}}}{2}.
\end{aligned} \tag{53}$$

With material parameters as described in Section 4, Table 1, and for $a = 5\,\mathrm{mm}$, $b = 10\,\mathrm{mm}$ and a reaction front positioned at $\rho = 9\,\mathrm{mm}$, the distribution of stresses and strains along the radius are shown in Figure 12 and Figure 13, respectively.

The strains at the reaction front are substituted into the expression (27) for χ. Then $\chi(\boldsymbol{\varepsilon}_+, T)$ in the case of this axially symmetric problem takes the form

$$\begin{aligned}
\chi(\boldsymbol{\varepsilon}_+, T) =& \frac{n_- M_-}{\rho_-}\left(\gamma(T) + \frac{1}{2}(\lambda_+ + \mu_+)(\varepsilon^{\mathrm{ch}})^2 + \frac{1}{2}\left([\![\lambda]\!](\varepsilon_r^+ + \varepsilon_\phi^+)^2 + 2[\![\mu]\!]((\varepsilon_r^+)^2 + (\varepsilon_\phi^+)^2)\right)\right. \\
&\left. -(\varepsilon_r^+ + \varepsilon_\phi^+)\varepsilon^{\mathrm{ch}}(\lambda_+ + \mu_+) + \frac{1 - 2\nu_-}{4\mu_-(1 - \nu_-)}\left([\![\lambda]\!](\varepsilon_r^+ + \varepsilon_\phi^+) + 2[\![\mu]\!]\varepsilon_r^+ - (\lambda_+ + \mu_+)\varepsilon^{\mathrm{ch}}\right)^2\right)
\end{aligned} \tag{54}$$

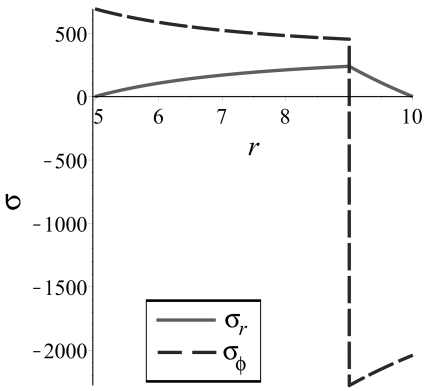

Figure 12: Distribution of stresses along the radius

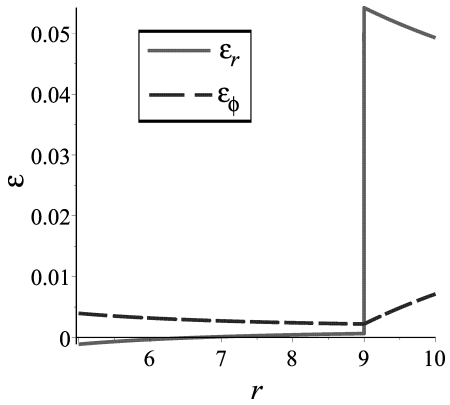

Figure 13: Distribution strains along the radius

with the strains which satisfy the equalities

$$\varepsilon_r^+ + \varepsilon_\phi^+ = 2A_+, \quad (\varepsilon_r^+)^2 + (\varepsilon_\phi^+)^2 = 2\left(A_+^2 + \frac{B_+^2}{\rho^4}\right), \tag{55}$$

and with the dependencies of A_+ and B_+ on ρ given by formulae (53). Then the equilibrium concentration $c_{\rm eq}$ of the diffusive constituent in dependence on the reaction front position ρ can be calculated by Eq. (26).

1.2 Diffusion Problem

Stationary diffusion is considered. The corresponding diffusion equation in the case of axial symmetry becomes:

$$\frac{\mathrm{d}}{\mathrm{d}r}\left(\frac{1}{r}\frac{\mathrm{d}c}{\mathrm{d}r}\right) = 0, \quad r \in [\rho, b]. \tag{56}$$

Boundary and interface conditions according to the notation of Figure 5 can be written as follows (as described in Section 2):

$$D\frac{\mathrm{d}c}{\mathrm{d}r}\bigg|_{r=b} - \alpha(c_* - c(b)) = 0, \qquad D\frac{\mathrm{d}c}{\mathrm{d}r}\bigg|_{r=\rho} - k_*\left(c(\rho) - c_{\rm eq}(\rho)\right) = 0. \tag{57}$$

In a cylindrical coordinate system the solution of the Laplace equation can be found as follows:

$$c(r) = C_1 \ln\left(\frac{r}{b}\right) + C_2. \tag{58}$$

The two unknown constants C_1 and C_2 can be found uniquely from the boundary conditions (57):

$$\begin{aligned} C_1 &= \frac{c_{\rm eq} - c_*}{\ln\dfrac{\rho}{b} - D\left(\dfrac{1}{k_*\rho} + \dfrac{1}{\alpha b}\right)}, \\ C_2 &= c_* - \frac{D}{\alpha b}C_1. \end{aligned} \tag{59}$$

From (58), (59) it follows that

$$c(\rho) = \frac{1}{\ln\dfrac{\rho}{b} - D\left(\dfrac{1}{k_*\rho} + \dfrac{1}{\alpha b}\right)}\left\{\left(\ln\frac{\rho}{b} - \frac{D}{\alpha b}\right)c_{eq}(\rho) - \frac{D}{k_*\rho}c_*\right\} \tag{60}$$

1.3 Reaction front kinetics

Since the normal component of the reaction front velocity is

$$W = -\frac{\mathrm{d}\rho}{\mathrm{d}t}, \tag{61}$$

the reaction front kinetics – the dependence $\rho(t)$ – can be obtained by integration of Eq. (31), which takes the above mentioned form (45):

$$\frac{d\rho}{dt} = -\frac{n_- M_-}{\rho_-} k_* \left(c(\rho) - c_{\rm eq}(\rho)\right). \tag{62}$$

where the dependencies $c(\rho)$ and $c_{\rm eq}(\rho)$ are already found.

It was shown earlier that the comparison of the values c_{eq} and c_* may be a tool for preliminary predictions of the reaction front behavior (Freidin et al. (2014, 2015)). Indeed, from Eq. (62) it follows that the direct reaction can go only if $c(\rho) > c_{\rm eq}(\rho)$. Since $c(b) < c_*$ and $c(b) \geq c(\rho)$, the front can propagate only if $c_{eq} < c_*$.

From (26) it follows that if $\chi(\varepsilon_+(\rho), T) = 0$ at some $\rho = \rho_* \in (a, b)$ then $c_{eq}(\rho_*) = c_*$ and, by (60), $c(\rho_*) = c_*$. Then $c(r) = c_*$ $r \in [\rho_*, b]$, and, by (62), the reaction front velocity $W = 0$. This case was shown by numerical simulation in Figure 7.

References

Buttner, C.; M.Zacharias: Retarded oxidation of si nanowires. *Appllied Phys. Lett.*, 89.

Chang, S.; Moon, J.; Cho, M.: Stress-diffusion coupled multiscale analysis of Si anode for Li-ion battery. *Journal of Mechanical Science and Technology*, 29(11), (2015), 4807–4816.

Cox, M.: The numerical evaluation of B-splines. Tech. rep., National Physics Laboratory DNAC 4 (1971).

Cui, Z.; Gao, F.; Qu, J.: A finite deformation stress-dependent chemical potential and its applications to lithium ion batteries. *Journal of the Mechanics and Physics of Solids*, 60, (2012a), 1280–1295.

Cui, Z.; Gao, F.; Qu, J.: Interface-reaction controlled diffusion in binary solids with applications to lithiation of silicon in lithium-ion batteries. *Journal of the Mechanics and Physics of Solids*, 61, (2012b), 293–310.

De Boor, C.: On calculation with B-splines. *Journal of Approximation Theory*, 6, (1972), 50–62.

De Lorenzis, L.; Wriggers, P.; Hughes, T.: Isogeometric contact: a review. *GAMM-Mitteilungen*, 37, (2014), 85–123.

Deal, E.; Grove, A.: General relationship for the thermal oxidation of silicon. *Applied Physics*, 36, (1965), 3770–3778.

Freidin, A.; Morozov, N.; Petrenko, S.; Vilchevskaya, E.; Korelev, I.: Chemical reactions in spherically-symmetric problems of mechanochemistry. *Acta Mechanica*, 227(1), (2015), 43–56.

Freidin, A. B.: Crazes and shear bands in glassy polymer as layers of a new phase. *Mechanics of Composite Materials*, 1, (1989), 1–7.

Freidin, A. B.: On new phase inclusions in elastic solids. *ZAMM Z. Angew. Math. Mech.*, 81, 2, (2007), 102–116.

Freidin, A. B.: On chemical reaction fronts in nonlinear elastic solids. In: D. Indeitsev; A. M. Krivtsov, eds., *Proceedings of XXXVII International Summer School-Conference Advanced Problems in Mechanics*, pages 231–237 (2009).

Freidin, A. B.: Chemical affinity tensor and stress-assist chemical reactions front propagation in solids. In: *Proceedings of the ASME 2013 International Mechanical Engineering Congress and Exposition*, vol. 9, page V009T10A102, American Society of Mechanical Engineers (2013).

Freidin, A. B.: On the chemical affinity tensor for chemical reactions in deformable materials. *Mechanics of Solids*, 50, 3, (2015), 260–285.

Freidin, A. B.; Korolev, I. K.; Aleshchenko, S. P.; Vilchevskaya, E. N.: Chemical affinity tensor and chemical reaction front propagation: theory and FE-simulations. *International journal of Fracture*, 202, (2016), 245–259.

Freidin, A. B.; Vilchevskaya, E. N.; Korolev, I.: Stress-assist chemical reactions front propagation in deformable solids. *International Journal of Engineering Science*, 83, (2014), 57–75.

Glansdorff, P.; Prigogine, I.: *Thermodynamic theory of stability and fluctuation*. Wiley-interscience, New-York (1971).

Grinfeld, M.: *Thermodynamic methods in the theory of heterogeneous systems*. Longman Sc & Tech (1991).

Gross, D.; Mueller, R.; Kolling, S.: Configurational forces - morphology evolution and finite elements. *Mechanics Research Communications*, 29, (2002), 529–536.

Hansbo, P.: Nitsche's method for interface problems in computa-tional mechanics. *GAMM-Mitteilungen*, 28, 2, (2005), 183–206.

Hughes, T.; Cottrell, J.; Bazilevs, Y.: Isogeometric analysis: CAD, finite elements, NURBS, exact geometry and mesh refinement. *Computer Methods in Applied Mechanics and Engineering*, 194, (2005), 4135–4195.

Jia, Z.; Li, T.: Stress-modulated driving force for lithiation reaction in hollow nano-anodes. *Journal of Power Sources*, 275, (2015), 866–876.

Juntunen, M.; Stenberg, R.: Nitsche's method for general boundary conditions. *Mathematics of Computation*, 78, 267, (2009), 1353–1374.

Kasavajjula, U.; Wang, C.; J. Appleby, A.: Nano- and bulk-silicon-based insertion anodes for lithium-ion secondary cells. *Journal of Power Sources*, 163, (2007), 1003–1039.

Khakalo, S.; Niiranen, J.: Isogeometric analysis of higher-order gradient elasticity by user elements of a commercial finite element software. *Computer-Aided Design*, 82, (2017), 154–169.

Kiendl, J.; Beltzinger, K.; Wüchner, R.: Isogeometric shell analysis with kirchhofflove elements. *Computer Methods in Applied Mechanics and Engineering*, 198, (2009), 3902–3914.

Kubanov, L.; Freidin, A.: Solid phase seeds in a deformable material. *J Appl Math Mech*, 52, (1988), 382–389.

Kunin, I.: *Elastic media with microstructure*. Springer, Berlin (1983).

Levitas, V.; Hamed, A.: Anisotropic compositional expansion and chemical potential for amorphous lithiated silicon under stress tensor. *Scientific Reports*, 3:1615.

Liu, X. H.; Fan, F.; Yang, H.; Zhang, S.; Huang, J. Y.; Zhu, T.: Self-limiting lithiation in silicon nanowires. *ACSNANO*, 7, 2, (2013), 1495–1503.

Liu, X. H.; Wang, J. W.; Huang, S.; Fan, F.; Huang, X.; Liu, Y.; Krylyuk, S.; Yoo, J.; Dayeh, S. A.; Davydov, A. V.; Mao, S. X.; Picraux, S. T.; Zhang, S.; Li, J.; Zhu, T.; Huang, J. Y.: In situ atomic-scale imaging of electrochemical lithiation in silicon. *Nature Nanotechnology*, 7, (2012a), 749–756.

Liu, X. H.; Zhong, L.; Huang, S.; Mao, S. X.; Zhu, T.; Huang, J. Y.: Size-dependent fracture of silicon nanoparticles during lithiation. *ACSNANO*, 6, 2, (2012b), 1522–1531.

Manni, C.; Pelosi, F.; Sampoli, M. L.: Isogeometric analysis in advectiondiffusion problems: Tension splines approximation. *Journal of Computational and Applied Mathematics*, 236, (2011), 511–528.

McDowell, M. T.; Lee, S. W.; Harris, J. T.; Korgel, B. A.; Wang, C.; Nix, W. D.; Cui, Y.: In situ TEM of two-phase lithiation of amorphous silicon nanospheres. *Nano letters*, 13, (2013), 758–764.

Morganti, S.; Auricchio, F.; Benson, D.; Gambarin, F.; Hartmann, S.; Hughes, T.; Reali, A.: Patient-specific isogeometric structural analysis of aortic valve closure. *Computer Methods in Applied Mechanics and Engineering*, 284, (2015), 508–520.

Morozov, N. F.; Freidin, A. B.: Phase transition zones and phase transformations of elastic solids under different stress states. *Proc. Steklov Mathe. Inst.*, 223, (1998), 220–232.

Mueller, R.; Gross, D.: 3D simulation of equilibrium morphologies of precipitates. *Computational Materials Science*, 11, (1998), 35–44.

Mueller, R.; Gross, D.: 3D inhomogeneous, misfitting second phase particles equilibrium shapes and morphological development. *Computational Materials Science*, 16, (1999), 53–60.

Mueller, R.; Gross, D.; Lupascu, D.: Driving forces on domain walls in ferroelectric materials and interaction with defects. *Computational Materials Science*, 35, (2006), 42–52.

Muhlstein, C.; Brown, S.; Ritchie, R.: High-cycle fatigue and durability of polycrystalline silicon thin films in ambient air. *Sens Actuators*, A94, (2002), 177–188.

Muhlstein, C.; Ritchie, R.: High-cycle fatigue of micronscale polycrystalline silicon films: fracture mechanics analyses of the role of the silica/silicon interface. *Int J Fract*, 119/120, (2003), 449–474.

Muhlstein, C.; Stach, E.; Ritchie, R.: A reaction-layer mechanism for the delayed failure of micron-scale polycrystalline silicon structural films subjected to high-cycle fatigue loading. *Acta Mater*, 50, (2001), 3579–3595.

Müller, W. H.; Vilchevskaya, E. N.; Freidin, A. B.: Structural changes in micro-materials: Phenomenology, theory, applications, and simulations. *Lecture Notes of TICMI*, 16, (2015), 3–72.

Niiranen, J.; Balobanov, V.; Kiendl, J.; Hosseini, S.: Variational formulations, model comparisons and isogeometric analysis for EulerBernoulli micro- and nano-beam models of strain gradient elasticity. *to appear in Mathematics and Mechanics of Solids*.

Niiranen, J.; Khakalo, S.; Balobanov, V.; Niemi, A.: Variational formulation and isogeometric analysis for fourth-order boundary value problems of gradient-elastic bar and plane strain/stress problems. *Computer Methods in Applied Mechanics and Engineering*, 308, (2016), 182–211.

Niiranen, J.; Kiendl, J.; Niemi, A.; Reali, A.: Isogeometric analysis for sixth-order boundary value problems of gradient-elastic kirchhoff plates. *Computer Methods in Applied Mechanics and Engineering*, 316, (2017b), 328–348.

Niiranen, J.; Niemi, A. H.: Variational formulations and general boundary conditions for sixth-order boundary value problems of gradient-elastic kirchhoff plates. *European Journal of Mechanics - A/Solids*, 61, (2017), 164–179.

Prigogine, I.; Defay, R.: *Chemical thermodynamics*. Longmans, Green (1954).

Rusanov, A. I.: Surface thermodynamics revisited. *Surface Science Reports*, 58, 5-8, (2005), 111–239.

Rusanov, A. I.: *Thermodynamic foundations of mechanochemistry*. Nauka, St. Petersburg (2006), in Russian.

Vilchevskaya, E.; Freidin, A.: Modelling mechanochemistry of the diffusion controlled chemical reaction front propagation in elastic solids. In: D. Indeitsev; A. M. Krivtsov, eds., *Proceedings of XXXVII Summer School-conference Advanced Problems in Mechanics (APM-2009), June 30 - July 5, 2009*, pages 741–749, Institute for Problems in Mechanical Engineering of Russian Academy of Science, St.Petersburg Russia (2009).

Vilchevskaya, E. N.; Freidin, A. B.: On kinetics of chemical reaction fronts in elastic solids. In: H. Altenbach; N. F. Morozov, eds., *Surface Effects in Solid Mechanics*, pages 181–194, Springer Berlin Heidelberg (2013).

Yang, F.: Effect of local solid reaction on diffusion-induced stress. *Journal of Applied Physics*, 107.

Zenga, Z.; Liu, N.; Zeng, Q.; Lee, S. W.; Mao, W. L.; Cui, Y.: In situ measurement of lithiation-induced stress in silicon nanoparticles using micro-raman spectroscopy. *Nano Energy*, 22, (2016), 105–110.

Address: Institute of Mechanics, Faculty of Mechanical Engineering, Berlin Institute of Technology, Einsteinufer 5, 10587 Berlin, Germany
email: mr.aleksandr.morozov@gmail.com